Discovery of WASP-174b: Doppler tomography of a near-grazing transit

L.Y. Temple,[1][⋆] C. Hellier,[1] Y. Almleaky,[2,3] D.R. Anderson,[1] F. Bouchy,[4] D.J.A. Brown,[5,6] A. Burdanov,[8] A. Collier Cameron,[7] L. Delrez,[9] M. Gillon,[8] R. Hall,[9] E. Jehin,[8] M. Lendl,[10,4] P.F.L. Maxted,[1] L. D. Nielsen,[4] F. Pepe,[4] D. Pollacco,[5,6] D. Queloz,[9] D. Ségransan,[4] B. Smalley,[1] S. Sohy,[8] S. Thompson,[9] A.H.M.J. Triaud,[11] O.D. Turner,[4,1] S. Udry,[4] R.G. West[5]

[1] *Astrophysics Group, Keele University, Staffordshire, ST5 5BG, UK*
[2] *Space and Astronomy Department, Faculty of Science, King Abdulaziz University, 21589 Jeddah, Saudi Arabia*
[3] *King Abdullah Centre for Crescent Observations and Astronomy (KACCOA), Makkah Clock, Saudia Arabia*
[4] *Observatoire astronomique de l'Université de Genève 51 ch. des Maillettes, 1290 Sauverny, Switzerland*
[5] *Department of Physics, University of Warwick, Gibbet Hill Road, Coventry, CV4 7AL, UK*
[6] *Centre for Exoplanets and Habitability, University of Warwick, Gibbet Hill Road, Coventry CV4 7AL, UK*
[7] *SUPA, School of Physics and Astronomy, University of St. Andrews, North Haugh, Fife, KY16 9SS, UK*
[8] *Space sciences, Technologies and Astrophysics Research (STAR) Institute, Université de Liège, Allée du 6 Août 17, 4000 Liège, Belgium*
[9] *Cavendish Laboratory, J J Thomson Avenue, Cambridge, CB3 0HE, UK*
[10] *Space Research Institute, Austrian Academy of Sciences, Schmiedlstr. 6, 80 42, Graz, Austria*
[11] *School of Physics & Astronomy, University of Birmingham, Edgbaston, Birmingham, B15 2TT, UK*

ABSTRACT

We report the discovery and tomographic detection of WASP-174b, a planet with a near-grazing transit on a 4.23-d orbit around a $V = 11.9$, F6V star with $[\text{Fe/H}] = 0.09 \pm 0.09$. The planet is in a moderately misaligned orbit with a sky-projected spin–orbit angle of $\lambda = 31° \pm 1°$. This is in agreement with the known tendency for orbits around hotter stars to be misaligned. Owing to the grazing transit the planet's radius is uncertain, with a possible range of 0.7–$1.7\,\text{R}_{\text{Jup}}$. The planet's mass has an upper limit of $1.3\,\text{M}_{\text{Jup}}$. WASP-174 is the faintest hot-Jupiter system so far confirmed by tomographic means.

Key words: techniques: spectroscopic – techniques: photometric – planetary systems – planets and satellites: individual – stars: individual – stars: rotation.

1 INTRODUCTION

Hot-Jupiter exoplanets orbiting hot, early-type stars have different properties from those orbiting cooler stars. First, they will be more highly irradiated, producing hotter atmospheres. The high irradiation is also thought to be related to the inflated radii seen in many hot Jupiters (e.g. Hartman et al. 2016). Second, hot Jupiters transiting hotter stars are more likely to be in misaligned orbits, a trait which has been discussed at length in recent literature (e.g. Valsecchi & Rasio 2014; Mazeh et al. 2015; Dai & Winn 2017, for a review, see Triaud (2017)). Further, where early-type stars are fast rotators, the rotation period can be shorter than the planet's orbital period, giving a systematically different tidal interaction than in most hot-Jupiter systems (see, e.g., Crouzet et al. 2017).

Hot, fast-rotating stars, however, usually give poor radial-velocity measurements owing to their broad and weak spectral lines. This means that planets around such stars are often confirmed by Doppler tomography of the stellar line profiles through a transit. The first planet discovered in this way was WASP-33b (Collier Cameron et al. 2010b), while recently such discoveries include: XO-6b (Crouzet et al. 2017), KELT-17b (Zhou et al. 2016a), KELT-9b (Gaudi et al. 2017), KELT-19Ab (Siverd et al. 2017), KELT-20b/MASCARA-2b (Lund et al. 2017; Talens et al. 2017a), KELT-21b (Johnson et al. 2017), HAT-P-57b (Hartman et al. 2015), HAT-P-67b (Zhou et al. 2017), Kepler-

448b (Bourrier et al. 2015), WASP-167b/KELT-13b (Temple et al. 2017) and MASCARA-1b (Talens et al. 2017b).

We report here the discovery of a hot Jupiter found as a candidate in the WASP-South transit survey (Hellier et al. 2011) and confirmed by Doppler tomography using the ESO 3.6-m/HARPS spectrograph (Pepe et al. 2002), together with follow-up photometry from the TRAPPIST-South and SPECULOOS Southern Observatory telescopes (Jehin et al. 2011; Burdanov et al. 2017).

2 OBSERVATIONS

The discovery photometry for WASP-174b was obtained using WASP-South, an array of eight cameras based at the South African Astronomical Observatory (SAAO), from 2006 May–2012 June. We used 30-s exposures and typically 10-minute cadence with a 400–700 nm broad-band filter. WASP-South data are reduced as explained by Collier Cameron et al. (2006) while the candidate selection process is explained by Collier Cameron et al. (2007).

Following the detection of a planet-like transit signal with a ∼ 4-day period we obtained two transit lightcurves using TRAPPIST-South and one using SPECULOOS-Europa (Section 2.1).

We obtained 16 radial-velocity measurements using the Euler/CORALIE spectrograph (Queloz et al. 2001). However, the broad spectral features meant that the error bars were large and thus the CORALIE data were not sufficient to confirm the planetary nature of the transiting object. We therefore decided to also use Doppler tomography, and observed a series of 23 spectra through transit with the HARPS spectrograph, taken simultaneously with one of the follow-up lightcurves on the night of Mar 13th 2016. Details of the observations are given in Table 1 while the measured radial velocities are given in Table 2.

We performed a search of the WASP discovery photometry looking for stellar rotational modulation of 0-1.5 cycles day^{-1}, using the methods of Maxted et al. (2011). We did not detect any modulations, with an upper limit of 0.8 mmag.

2.1 The SPECULOOS-Europa telescope

The SPECULOOS-Europa telescope is one of four identical telescopes which form the SPECULOOS Southern Observatory currently being installed at ESO Paranal Observatory. SPECULOOS is a ground-based transit survey that will search for Earth-sized planets transiting the nearest ultracool dwarfs (Burdanov et al. (2017)). Each SPECULOOS telescope is a robotic Ritchey-Chretien (F/8) telescope of 1-m diameter. They are equipped with Andor Peltier-cooled deeply depleted 2K×2K CCD cameras, with 13.5 micron pixels. The field of view of each telescope is 12' × 12' and the corresponding pixel scale is 0.35"pixel^{-1}. WASP-174b was observed with 10-sec exposure times in an I+z' band on the night of 13th July 2017.

3 SPECTRAL ANALYSIS

We first performed a spectral analysis on a median-stacked HARPS spectrum created from the 23 we obtained, in order

Table 1. Details of all observations of WASP-174b used in this work, including the discovery photometry, the follow-up photometry and the spectroscopic observations.

Facility	Date	Notes
WASP-South	2006 May–2012 Jun	35883 points
TRAPPIST-South	2016-03-13	I+z'. 8s exp.
TRAPPIST-South	2017-03-08	V. 15s exp.
SPECULOOS-Europa	2017-07-13	I+z'. 10s exp.
CORALIE	Mar 2014 – Aug 2017	16 out-of-transit spectra
HARPS	2016-03-13	23 in-transit spectra

Table 2. Radial velocities and bisector spans for WASP-174b.

BJD (UTC −2,450,000)	RV (km s^{-1})	$\sigma_{\rm RV}$ (km s^{-1})	BS (km s^{-1})	$\sigma_{\rm BS}$ (km s^{-1})
CORALIE RVs:				
6719.750940	4.87	0.05	12.39	0.10
6770.634386	4.91	0.05	12.01	0.10
6836.575290	4.84	0.09	11.97	0.18
7072.738390	4.71	0.06	12.64	0.12
7888.597085	4.79	0.09	13.14	0.18
7890.515148	4.73	0.14	13.29	0.28
7894.501754	4.79	0.08	13.24	0.16
7903.604885	4.66	0.13	13.29	0.26
7905.688333	4.85	0.07	13.12	0.14
7917.567196	4.85	0.07	13.05	0.14
7924.504883	4.82	0.06	13.07	0.12
7951.505749	4.73	0.17	13.10	0.34
7954.494322	4.83	0.07	13.31	0.14
7959.516253	4.70	0.09	13.12	0.18
7973.491791	4.82	0.12	12.67	0.24
7974.518063	4.65	0.09	12.91	0.18
HARPS in-transit RVs:				
7461.571827	4.873	0.02	−0.09	0.04
7461.582499	4.889	0.02	−0.16	0.04
7461.593380	4.877	0.02	−0.09	0.04
7461.604248	4.851	0.02	−0.16	0.04
7461.615140	4.885	0.02	−0.15	0.04
7461.625708	4.862	0.02	−0.10	0.04
7461.636692	4.854	0.02	−0.12	0.04
7461.647260	4.889	0.02	−0.10	0.04
7461.657920	4.859	0.02	−0.03	0.04
7461.668696	4.878	0.02	−0.14	0.04
7461.679576	4.832	0.02	−0.09	0.04
7461.690352	4.783	0.02	0.12	0.04
7461.701024	4.767	0.01	0.07	0.02
7461.711800	4.792	0.01	−0.03	0.02
7461.722576	4.782	0.02	−0.13	0.04
7461.733457	4.812	0.01	−0.15	0.02
7461.743804	4.829	0.02	−0.10	0.04
7461.754893	4.843	0.02	−0.00	0.04
7461.765565	4.884	0.02	−0.10	0.04
7461.776549	4.852	0.02	−0.19	0.04
7461.787013	4.869	0.02	−0.15	0.04
7461.797985	4.867	0.02	−0.02	0.04

to determine some stellar properties. We follow the method described by Doyle et al. (2013) to determine values for the stellar effective temperature T_{eff}, the stellar metallicity [Fe/H], the stellar lithium abundance $\log A(\text{Li})$ and the projected stellar rotational velocity $v \sin i_{\star}$. To constrain the latter we obtain a macroturbulence value of 6.3 km s^{-1} using the Doyle et al. (2014) calibration. We also determine the spectral type of the star to be F6V, by using the MKCLASS program (Gray & Corbally 2014). Due to the star being of an early spectral type and a rapid rotator the spectra contain few and broad lines, and so we were unable to determine a value for the stellar surface gravity $\log g_{\star}$. Thus we instead assumed a value of $\log g_{\star} = 4.0$. The values obtained for each of the fitted parameters are given in Table 3.

4   COMBINED ANALYSES

We performed a Markov Chain Monte Carlo (MCMC) fitting procedure which uses the stellar parameters obtained in the spectral analysis (Section 3) to constrain the fit. We used the latest version of the MCMC code described by Collier Cameron et al. (2007) and Pollacco et al. (2008), which is capable of fitting photometric, RV and tomographic data simultaneously (Collier Cameron et al. 2010a).

The system parameters which are determined from the photometric data are the epoch of mid-transit T_{c}, the orbital period P, the planet-to-star area ratio $(R_{\text{p}}/R_{\star})^2$, the transit duration T_{14}, and the impact parameter b. Limb darkening was accounted for using the Claret (2000, 2004) four-parameter non-linear law. The proposed values of the stellar mass are calculated using the Enoch–Torres relation (Enoch et al. 2010; Torres et al. 2010).

The RV fitting then provides values for the stellar reflex velocity semi-amplitude K_1 and the barycentric system velocity γ. We assume a circular orbit, since we do not have sufficient quantity or quality in the out-of-transit RVs to constrain the eccentricity. In any case, hot Jupiters often settle into circular orbits on time-scales that are shorter than their lifetimes through tidal circularization (Pont et al. 2011), so usually their orbits are circular. If there are accurate RVs taken through transit, it is also possible to measure the projected spin-orbit misalignment angle λ by fitting the Rossiter–McLaughlin (RM) effect.

The 23 HARPS spectra were cross-correlated using the standard HARPS Data Reduction Software over a window of $\pm 350 \text{ km s}^{-1}$ (as described in Baranne et al. (1996), Pepe et al. (2002)). The cross-correlation functions (CCFs) were created using a mask matching a G2 spectral type, containing zeroes at the positions of absorption lines and ones in the continuum. The tomographic data are then comprised of the time series of CCFs taken through transit.

We used the MCMC code in two modes. The first mode fits the CCFs to obtain RV values, and then uses the calibrations of Hirano et al. (2011) to model the RM effect and thus measure λ. The second mode fits the CCFs directly, modelling the in-transit perturbations of the CCFs due to the path of the planet across the stellar disc (e.g. Brown et al. 2017; Temple et al. 2017). The parameters determined in this part of the analysis are $v \sin i_{\star}$, λ, the stellar line-profile Full-Width at Half-Maximum (FWHM), the FWHM of the line perturbation due to the planet v_{FWHM} and the system
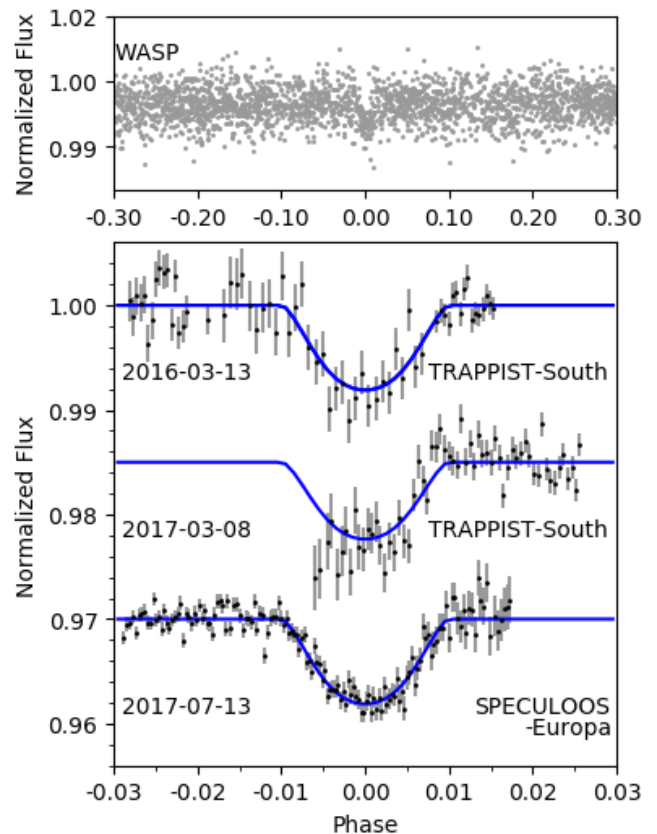
Figure 1. The WASP discovery photometry (top) and follow-up transit lightcurves (bottom). The blue lines show the final model obtained in the MCMC fitting (see Section 4).

γ-velocity. The MCMC code assumes a Gaussian shape for the line perturbation caused by the planet. We obtain initial values for the stellar line FWHM and the γ-velocity by fitting a Gaussian profile to the CCFs and apply the spectral $v \sin i_{\star}$ and T_{eff} as priors. Neither λ nor v_{FWHM} had a prior applied.

We give the adopted solution to the photometry and RV fitting and then compare the results of fitting λ via the two methods in Table 3. We adopt the value of λ from fitting the CCFs since it is a more direct method that uses more of the line-profile information.

4.1   A grazing transit

The photometry and the best-fitting model are shown in Fig. 1. We found that constraining the photometric fit was difficult since the transit is either grazing or near-grazing and does not show clear 2nd and 3rd contacts. This means that R_{p}, R_{*} and the impact parameter b are poorly constrained. We adopt the solution to the photometry obtained by the first MCMC run (which included the photometry, RVs and an RM fit). We then show the probability distributions of these parameters in Fig. 2. This reveals that we cannot distinguish between grazing and near-grazing solutions.
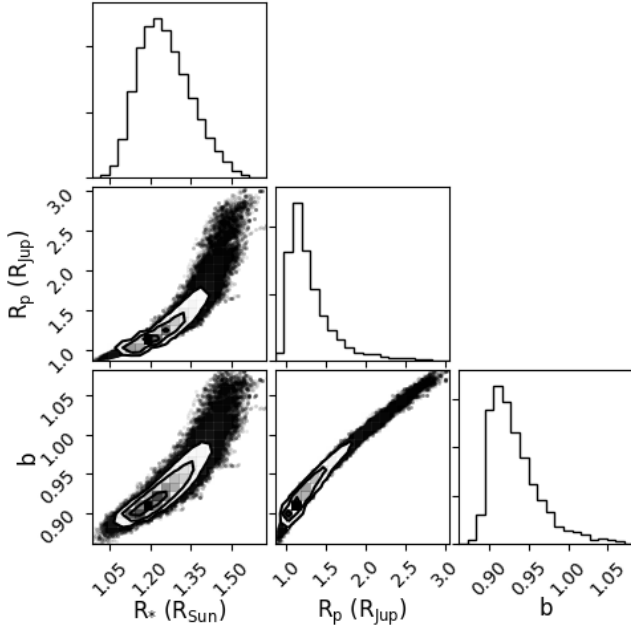
Figure 2. Probability distributions for the parameters R_p, R_* and b, created from the results of the first-mode MCMC run. We calculated a "grazing criterion" for the distribution of proposed values by taking the median of the quantity $(R_p/R_* + b)$, which if > 1 implies a grazing orbit (Smalley et al. 2011). We obtain $1.02^{+0.04}_{-0.02}$: a grazing solution with the possibility of a non-grazing solution being within 1σ. Thus we cannot distinguish between a grazing or near-grazing solution.

4.2 The planet's mass

The CORALIE and HARPS RVs are shown in Fig. 3. Due to the relatively large error bars in the out-of-transit RV measurements we do not regard the fitted semi-amplitude to be a measure of the planet's mass. However, we were able to put a 95 % confidence upper limit on the mass of $1.3\,M_{Jup}$, and the predicted curve for this value is also shown in Fig. 3.

4.3 The Doppler track

We display the tomographic data as a function of the planet's orbital phase in Fig. 4. In constructing this plot we have first produced a "minimum CCF", which at each wavelength has the lowest value from the range of phases, and then subtracted this from each CCF in order to remove the invariant stellar line profile (following the method of Temple et al. (2017)). We also display the simultaneous photometric observation alongside.

We interpret the resulting tomogram as showing a faint, prograde-moving planet signal crossing only the red-shifted portion of the plot. This is in line with the transit being grazing, such that the planet crosses only a short chord on the face of the star (see Fig. 5).

The planet's Doppler shadow appears very faint at the beginning and end of the transit (see Fig. 4). This is likely due to there being little of the planet on the face of the star near 1st and 4th contacts, owing to the near-grazing nature of the orbit.

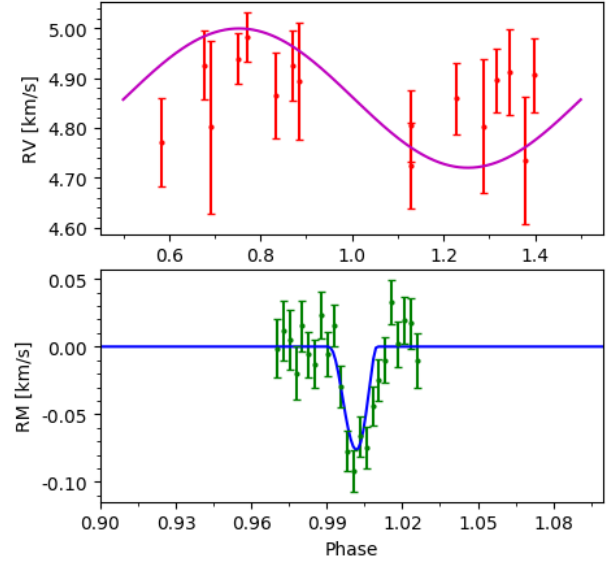**Figure 3.** Top: The 16 CORALIE RVs (red points) obtained for WASP-174b . The magenta line shows the expected RV amplitude for a planet of $1.3\,M_{Jup}$, our derived upper limit (95 % confidence). Bottom: the 23 in-transit HARPS RVs (green points). The blue line shows the best fit model with the Keplerian RV curve subtracted, leaving only the fit to the RM effect.

5 STELLAR AGE DETERMINATION

We estimated the age of WASP-174 using the open source software BAGEMASS[1]. BAGEMASS uses the Bayesian method of Maxted et al. (2015) to fit the age, mass and initial metallicity of a star using the GARSTEC stellar evolution code (Weiss & Schlattl 2008). We applied constraints on the stellar temperature and metallicity ($T_{eff} = 6400 \pm 100\,K$ and $[Fe/H] = 0.09 \pm 0.09$ as obtained in the spectral analysis) as well as the stellar density ($\rho_*/\rho_\odot = 0.6 \pm 0.2$ from the transit analysis). We adopt the solution obtained for a solar mixing length and He abundance, since enhancing the He abundance made no significant change to the fit while reducing the solar mixing length worsened the fit. We display the resulting isochrones and evolutionary tracks for this fit in Fig. 6 and the fitted values are given in Table 3.

We find WASP-174 to be consistent with a main-sequence star or one beginning to evolve off the main sequence. The Li abundance obtained in Section 3 is also consistent with the star being non-evolved, but for mid-F stars the Li abundance is not a good age indicator. For the measured value of $\log A(Li) = 2.48 \pm 0.10$, WASP-174 could be up to a few Gyr old (Sestito & Randich 2005).

6 DISCUSSION AND CONCLUSIONS

WASP-174b is revealed by Doppler tomography to be a planet making a grazing transit of its host star in a mis-aligned orbit with an alignment angle of $\lambda = 31° \pm 1°$.

WASP-174 is an F6 star with an effective temperature of
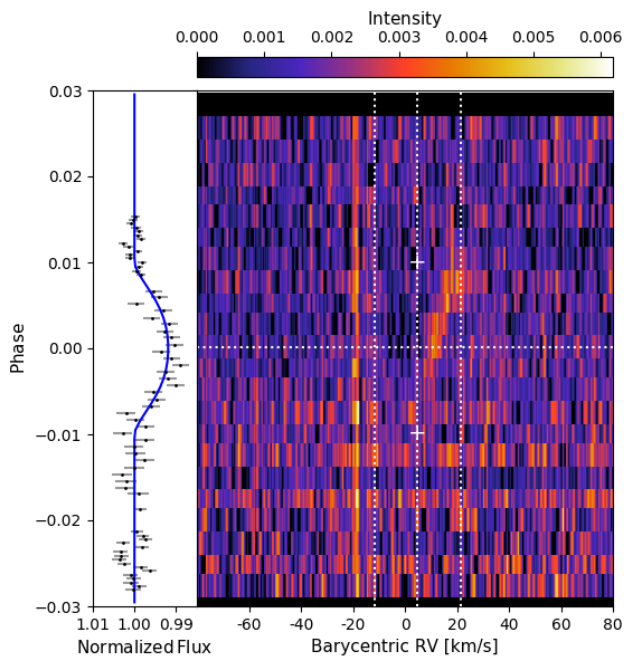
[1] http://sourceforge.net/projects/bagemass

Figure 4. The line profiles through transit, with the "minimum CCF" subtracted. The simultaneous TRAPPIST-South lightcurve is displayed alongside. We interpret this tomogram as showing a prograde-moving planet signal in the red-shifted section of the tomogram. This implies that the misaligned orbit is such that the planet only passes in front of the portion of the star which is moving away from us. The white dashed vertical lines mark the positions of the γ velocity of the system and the positions of $\gamma \pm v \sin i_\star$. The phase of mid-transit is marked by the white horizontal dashed line. The white $+$ symbols indicate the beginning and end of the transit event, calculated using the ephemeris obtained in the adopted solution to the photometry (see Section 4).
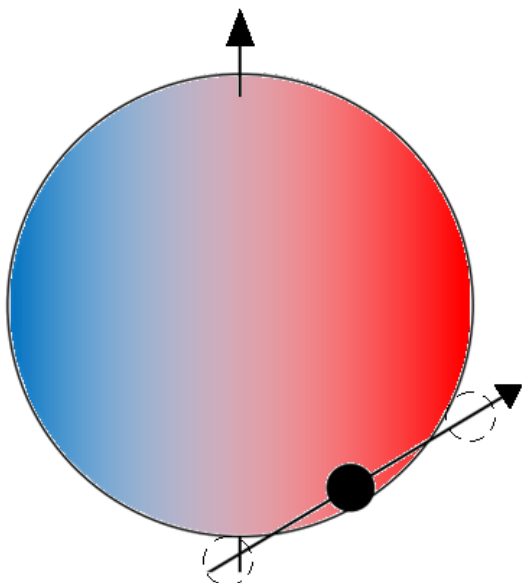
Figure 5. The transit chord calculated from the fitted values of R_p, $R_\star$, b and λ (see Table 3.) The dashed circles show the 1$^{\text{st}}$ and 4$^{\text{th}}$ contacts.
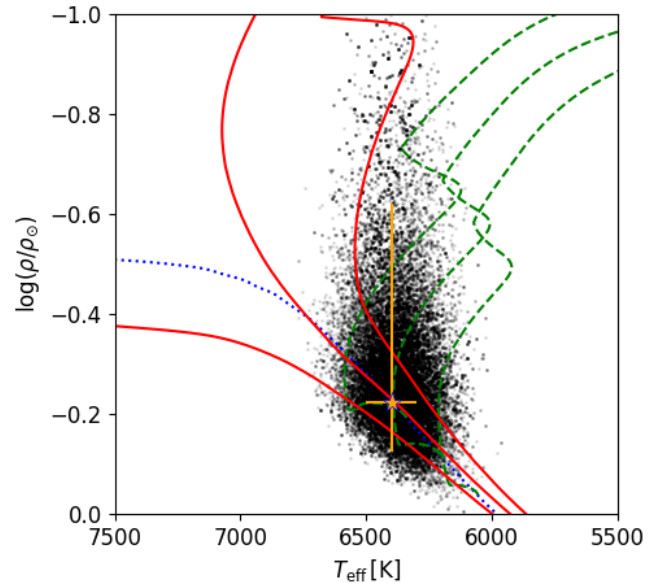
Figure 6. The best fitting evolutionary tracks and isochrones of WASP-174 obtained using BAGEMASS. Dotted blue line: ZAMS at best-fit [Fe/H]. Green dashed lines: evolutionary track for the best-fit [Fe/H] and mass, plus 1σ bounds. Red lines: isochrone for the best-fit [Fe/H] and age, plus 1σ bounds. Orange star: measured values of T_{eff} and $\rho_\star$ for WASP-174 obtained in the spectral and photometric analyses respectively.

$T_{\text{eff}} = 6400 \pm 100$ K, and is a fairly rapid rotator with a measured $v \sin i_\star$ of 16.5 ± 0.5 km s^{-1}. This rotation rate, together with a fitted radius of 1.3 ± 0.1 R$_\odot$, implies a stellar rotation period of $P_{\text{rot}} < 4.4$ d. Since the planet's orbital period is 4.23 d, this means that the stellar rotation period could be, but is not certain to be, shorter than the planet's orbit. Most hot-Jupiter systems have rotation periods that are longer than the orbit, but having $P_{\text{orb}} < P_{\text{rot}}$ has been found for other hot, rapidly rotating host stars, including KELT-17b (Zhou et al. 2016a), WASP-167b/KELT-13b (Temple et al. 2017) and XO-6b (Crouzet et al. 2017). In systems with $P_{\text{orb}} < P_{\text{rot}}$ and with prograde orbits the tidal interaction is thought to produce decay of the planet's orbit, but this will be reversed in systems such as WASP-174, with a prograde orbit and with $P_{\text{orb}} > P_{\text{rot}}$ (see the discussions in Crouzet et al. (2017) and Temple et al. (2017)). The difference in dynamical evolution of hot-star hot Jupiters is one reason for finding more examples of such systems.

Another dynamical difference is that hot-Jupiter orbits are much more likely to be misaligned around hotter stars, which might be related to reduced tidal damping in hotter stars with smaller or absent convective envelopes (Winn et al. 2010). With a misaligned orbit WASP-174b is in line with this trend. Of the 12 other systems confirmed with tomographic methods, 8 are at least moderately misaligned. These are WASP-33b (Collier Cameron et al. 2010b), HAT-P-57b (Hartman et al. 2015), KELT-17b (Zhou et al. 2016a), KELT-9b (Gaudi et al. 2017), KELT-19Ab (Siverd et al. 2017), XO-6b (Crouzet et al. 2017), WASP-167b/KELT-13b (Temple et al. 2017) and MASCARA-1b (Talens et al. 2017b).

High stellar irradiation produces hotter planetary atmospheres, and is thought to result in the inflated radii seen

Table 3. All system parameters obtained for WASP-174b in this work.

1SWASP J130310.57–412305.3
2MASS J13031055–4123053
RA = $13^h03^m10.57^s$, Dec = $-41°23'05.3''$ (J2000)
$V = 11.9$ (NOMAD)
IRFM $T_{eff} = 6417 \pm 142$ K
UCAC4 Proper Motions: (RA) 0.6 ± 0.8 (Dec) -5.9 ± 1.7 mas/yr
Rotational Modulations: < 0.8 mmag (95%)

Stellar parameters from spectral analysis:

Parameter (Unit)	Value
Spectral type	F6V
T_{eff} (K)	6400 ± 100
[Fe/H]	0.09 ± 0.09
$\log A(Li)$	2.48 ± 0.10
$v \sin i_*$ (km s^{-1})	16.5 ± 0.5
Macroturbulence (km s^{-1})	6.3 km s^{-1}

Parameters from photometric and RV analysis:

P (d)	4.233700 ± 0.000003
T_c (BJD$_{TDB}$)	2457465.9322 ± 0.0005
T_{14} (d)	0.084 ± 0.002
$\Delta F = R_P^2/R_*^2$	0.0089 ± 0.0003
b	0.92 ± 0.03
i (°)	84.5 ± 0.6
a (AU)	0.0555 ± 0.0009
M_* ($M_\odot$)	1.27 ± 0.06
R_* ($R_\odot$)	1.3 ± 0.1
$\log g_*$ (cgs)	4.35 ± 0.05
ρ_* ($\rho_\odot$)	0.6 ± 0.2
T_{eff} (K)	6400 ± 100
[Fe/H]	0.09 ± 0.09
M_P (M_{Jup})	< 1.3 (95%)
R_P (R_{Jup})	1.2 ± 0.5
T_{eql} (K)	1470 ± 60

Parameters from RM and DT analyses:

Parameter (Unit)	DT Value (adopted):	RM Value:
γ (km s^{-1})	4.8 ± 0.1	4.860 ± 0.004
λ (°)	31 ± 1	31 ± 4

Parameters from SED analysis:

Parameter (Unit)	Value
Age (Gyr)	1.65 ± 0.85
M_* ($M_\odot$)	1.28 ± 0.07
[Fe/H]$_{init}$	0.12 ± 0.08

in many hot Jupiters (e.g. Hartman et al. 2016; Zhou et al. 2017; Siverd et al. 2017). With an equilibrium temperature of 1470 ± 60 K, we would thus expect WASP-174b to be moderately inflated.

The actual planetary radius is hard to measure owing to the grazing or near-grazing transit, which means that 2nd and 3rd contacts are not visible in the transit profile and the fitted radius is degenerate with the impact parameter (Fig. 2). Thus we can do no better than loosely constraining the radius to $R_P = 1.2 \pm 0.5$ R$_{Jup}$, which is consistent with that of an inflated hot Jupiter.

The mass of WASP-174b is also uncertain, since the hot and rapidly-rotating host star limits the accuracy and precision of radial-velocity measurements. We report only an upper limit of 1.3 M$_{Jup}$, so again WASP-174b is most likely

a fairly typical inflated hot Jupiter. It may be possible, however, to constrain the mass further with some more precise RV measurements taken out-of-transit using HARPS.

At $V = 11.9$, WASP-174 is the faintest hot-Jupiter system for which the shadow of the planet has been detected by tomographic methods. The next faintest are Kepler-448 at $V = 11.4$ (Bourrier et al. 2015) and HAT-P-56 at $V = 10.9$ (Huang et al. 2015), which was initially confirmed with radial velocity measurements.

HAT-P-56b is also comparable in that it has a near-grazing transit with an impact parameter of $b = 0.873^{+0.004}_{-0.006}$ (Huang et al. 2015), which compares with $b = 0.92 \pm 0.03$ for WASP-174b . As with our work the tomographic planet trace for HAT-P-56b is faint and possibly shows evidence for getting fainter when the planet is only partially occulting the star (i.e. at the beginning and end of the transit, Zhou et al. 2016b).

REFERENCES

Baranne A., et al., 1996, A&AS, 119, 373
Bourrier V., et al., 2015, A&A, 579, A55
Brown D. J. A., et al., 2017, MNRAS, 464, 810
Burdanov A., Delrez L., Gillon M., Jehin E., 2017, preprint, (arXiv:1710.03775)
Claret A., 2000, A&A, 363, 1081
Claret A., 2004, A&A, 428, 1001
Collier Cameron A., et al., 2006, MNRAS, 373, 799
Collier Cameron A., et al., 2007, MNRAS, 380, 1230
Collier Cameron A., Bruce V. A., Miller G. R. M., Triaud A. H. M. J., Queloz D., 2010a, MNRAS, 403, 151
Collier Cameron A., et al., 2010b, MNRAS, 407, 507
Crouzet N., et al., 2017, AJ, 153, 94
Dai F., Winn J. N., 2017, AJ, 153, 205
Doyle A. P., et al., 2013, MNRAS, 428, 3164
Doyle A. P., Davies G. R., Smalley B., Chaplin W. J., Elsworth Y., 2014, MNRAS, 444, 3592
Enoch B., Collier Cameron A., Parley N. R., Hebb L., 2010, A&A, 516, A33
Gaudi B. S., et al., 2017, Nature, 546, 514

Gray R. O., Corbally C. J., 2014, AJ, 147, 80

Hartman J. D., et al., 2015, AJ, 150, 197

Hartman J. D., et al., 2016, AJ, 152, 182

Hellier C., et al., 2011, in European Physical Journal Web of Conferences. p. 01004 (arXiv:1012.2286), doi:10.1051/epjconf/20101101004

Hirano T., Suto Y., Winn J. N., Taruya A., Narita N., Albrecht S., Sato B., 2011, ApJ, 742, 69

Huang C. X., et al., 2015, AJ, 150, 85

Jehin E., et al., 2011, The Messenger, 145, 2

Johnson M. C., et al., 2017, preprint, (arXiv:1712.03241)

Lund M. B., et al., 2017, AJ, 154, 194

Maxted P. F. L., et al., 2011, PASP, 123, 547

Maxted P. F. L., Serenelli A. M., Southworth J., 2015, A&A, 575, A36

Mazeh T., Perets H. B., McQuillan A., Goldstein E. S., 2015, ApJ, 801, 3

Pepe F., et al., 2002, The Messenger, 110, 9

Pollacco D., et al., 2008, MNRAS, 385, 1576

Pont F., Husnoo N., Mazeh T., Fabrycky D., 2011, MNRAS, 414, 1278

Queloz D., et al., 2001, The Messenger, 105, 1

Sestito P., Randich S., 2005, A&A, 442, 615

Siverd R. J., et al., 2017, preprint, (arXiv:1709.07010)

Smalley B., et al., 2011, A&A, 526, A130

Talens G. J. J., et al., 2017a, preprint, (arXiv:1707.01500)

Talens G. J. J., et al., 2017b, A&A, 606, A73

Temple L. Y., et al., 2017, MNRAS, 471, 2743

Torres G., Andersen J., Giménez A., 2010, A&ARv, 18, 67

Triaud A. H. M. J., 2017, preprint, (arXiv:1709.06376)

Valsecchi F., Rasio F. A., 2014, ApJ, 786, 102

Weiss A., Schlattl H., 2008, Ap&SS, 316, 99

Winn J. N., Fabrycky D., Albrecht S., Johnson J. A., 2010, ApJ, 718, L145

Zhou G., et al., 2016a, AJ, 152, 136

Zhou G., Latham D. W., Bieryla A., Beatty T. G., Buchhave L. A., Esquerdo G. A., Berlind P., Calkins M. L., 2016b, MNRAS, 460, 3376

Zhou G., et al., 2017, AJ, 153, 211

de Wit J., Seager S., 2013, Science, 342, 1473

This paper has been typeset from a TeX/LaTeX file prepared by the author.